

Orientalional phase transitions in holmium orthoferrite with magnetic vacancies

G. P. Vorob'ev, A.M. Kadomtseva, I. B. Krynetskii, M. M. Lukina, and A. A. Mukhin

Institute of General Physics, Academy of Sciences of the USSR, Moscow;

M. V. Lomonosov State University, Moscow

(Submitted 6 November 1990)

Zh. Eksp. Teor. Fiz. **99**, 1319–1335 (April 1991)

The presence of nonmagnetic Al^{3+} impurity ions, i.e., of magnetic vacancies, in $\text{HoFe}_{1-x}\text{Al}_x\text{O}_3$ induces new unusual spontaneous and induced (by an external magnetic field) orientational phase transitions. A detailed theoretical analysis of the mechanisms of the observed phase transitions in $\text{HoFe}_{1-x}\text{Al}_x\text{O}_3$ was made. It was found that at low temperatures the application of magnetic fields $\mathbf{H} \parallel \mathbf{a}$ and $\mathbf{H} \parallel \mathbf{b}$ induced characteristic metamagnetic transitions in the Ho subsystem representing abrupt magnetization reversal in the rare-earth ions with a magnetic vacancy in their environment. These transitions were accompanied by orientational transitions in the d subsystem because of the f - d exchange interaction. In a field $\mathbf{H} \parallel \mathbf{a}$ such a metamagnetic transition in the Ho subsystem was accompanied by an orientational phase transition $\Gamma_{12}(G_y G_z F_x) - \Gamma_2(G_z F_x)$ in the d subsystem, which was manifested by an abrupt change in the magnetization and magnetostriction curves. A characteristic feature of the H_x - T phase diagram was the presence of a bicritical point at $T = 60$ K, where two lines representing second-order phase transitions ($\Gamma_2 - \Gamma_{12}$ and $\Gamma_{24} - \Gamma_2$) converged with a line representing a first-order phase transition ($\Gamma_{24} - \Gamma_{12}$). New orientational phase transitions were observed in a field $\mathbf{H} \parallel \mathbf{b}$ and included $\Gamma_{13} - \Gamma_{1234} - \Gamma_{34}$ transitions due to alternate magnetization reversal of the rare-earth ions at inequivalent positions magnetized by the effective field of the magnetic vacancies in the direction opposite to the external magnetic field. The effective field created by the magnetic vacancies at the Ho^{3+} ions was determined to be $H_{mv} \approx 25$ kOe.

Orthoferrites (RFeO_3) and orthochromites (RCrO_3) containing strongly anisotropic (Ising) rare-earth ions ($\text{R}^{3+} = \text{Dy}^{3+}, \text{Ho}^{3+}, \text{Tb}^{3+}$) exhibit magnetic behavior with a number of interesting features.¹⁻⁵ One of the most striking effects observed in these compounds is a giant change in the magnetic anisotropy under the influence of nonmagnetic impurity ions in the d subsystem (magnetic vacancies).^{1-4,5} An additional contribution to the anisotropy energy in these orthoferrites is made by the appearance at these rare-earth ions of a strong exchange field $H_{mv} \approx 10^4$ Oe due to decompensation of the f - d exchange near a magnetic vacancy. It was shown in Refs. 1 and 2 that, depending on the orientation of the Ising axis, this additional anisotropy may stabilize different magnetic configurations. For example, in the case of dysprosium and holmium orthoferrites, where the susceptibility was maximal along the \mathbf{b} axis, so that their Ising axis was in the \mathbf{ab} plane and oriented at an angle of $\sim 60^\circ$ to the \mathbf{a} axis, the contribution to the anisotropy made by such magnetic vacancies stabilized the $\Gamma_1(G_y)$ magnetic structure. In the case of dysprosium orthoferrite, which exhibited the $\Gamma_4 - \Gamma_1$ Morin spontaneous spin-reorientation transition, this gave rise to a larger shift of the transition temperature toward higher temperatures when the amount of Al^{3+} nonmagnetic impurity ions was increased.² An even stronger influence of the magnetic vacancies was observed in $\text{HoFe}_{1-x}\text{Al}_x\text{O}_3$ (Ref. 1), where a new (not observed in holmium orthoferrite) orientational transition to the antiferromagnetic state $\Gamma_1(G_y)$ took place. It should be noted that substituted holmium orthoferrite is an interesting material for the investigation because, as was shown earlier,^{6,7} contrary to the usual views the compound HoFeO_3 undergoes a complex $\Gamma_4 - \Gamma_{24} - \Gamma_{12} - \Gamma_2$ orientational transition, and it would be interesting to investigate how this transition is affected by the magnetic vacancies. Moreover, it

would be highly desirable to investigate not only the spontaneous but also the induced (by an external magnetic field) orientational transitions in $\text{HoFe}_{1-x}\text{Al}_x\text{O}_3$, since the induced transitions can give extensive information on various magnetic interactions in this compound.

EXPERIMENTAL RESULTS

We investigated magnetic and magnetoelastic properties of $\text{HoFe}_{1-x}\text{Al}_x\text{O}_3$ ($x = 0.03, 0.07$) single crystals grown by the method of spontaneous crystallization from a molten solution. The quantitative concentration of the Al^{3+} ions was determined by x-ray spectroscopic analysis to within 4%. The magnetization curves were recorded using a vibrating-sample magnetometer, and the magnetostriction isotherms were recorded using strain gauges in fields up to 50 and 42 kOe, respectively; the torque curves were obtained using a torsion magnetic balance in fields up to 12 kOe in a wide range of temperatures (1.8–100 K).

The magnetization curves recorded along the \mathbf{a} , \mathbf{b} , and \mathbf{c} axes (corresponding to the x , y , and z axes) of an $\text{HoFe}_{0.97}\text{Al}_{0.03}\text{O}_3$ crystal at 1.8 K are shown in Fig. 1a. Clearly, the magnetization is strongly anisotropic: it is maximal along the \mathbf{a} and \mathbf{b} axes and minimal along the \mathbf{c} axis of the crystal ($m_b > m_a \gg m_c$). In strong magnetic fields the magnetization reaches saturation along the \mathbf{b} and \mathbf{a} axes. The saturation values were $m_b = 164 \text{ G} \cdot \text{cm}^3 \cdot \text{g}^{-1}$ (corresponding to $8\mu_B$) and $m_a = 73 \text{ G} \cdot \text{cm}^3 \cdot \text{g}^{-1}$ ($3.65\mu_B$), respectively, whereas along the \mathbf{c} axis the magnetization depends linearly on the field and the susceptibility was $\chi_c = 4.5 \times 10^{-4} \text{ cm}^3/\text{g}$; moreover, measurements carried out at high temperatures indicated that χ_c varies little with temperature up to 55 K but had a maximum near $T = 60$ K, which was due to a spin reorientation transition in this range of tempera-

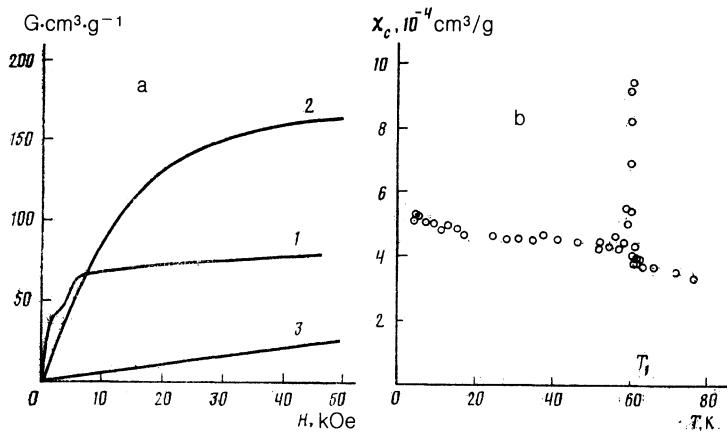


FIG. 1. a) Magnetization curves of $\text{HoFe}_{0.97}\text{Al}_{0.03}\text{O}_3$ at $T = 1.85$ K: 1) $\text{H} \parallel \text{a}$; 2) $\text{H} \parallel \text{b}$; 3) $\text{H} \parallel \text{c}$. b) Temperature dependence of the susceptibility of $\text{HoFe}_{0.97}\text{Al}_{0.03}\text{O}_3$ along the c axis.

tures (Fig. 1b). The magnetization curves recorded for a sample with composition $x = 0.07$ were also anisotropic and similar to those plotted in Fig. 1a.

It was shown earlier^{7,8} that similar magnetization curves are exhibited by pure holmium orthoferrite and orthochromite in which the Ho^{3+} ions are regarded as the Ising ions with the magnetic moment $m = 9\mu_B$ oriented in the ab plane at an angle $\alpha = 65^\circ$ to the a axis of the crystal. Consequently, the magnetic vacancies do not distort the Ising nature of the behavior of the Ho^{3+} ions in these compounds in which the Ising axis, as in the specific case of $\text{HoFe}_{0.97}\text{Al}_{0.03}\text{O}_3$ is oriented, according to our measurements, at the angle $\alpha = \tan^{-1}(m_b/m_a) = 65^\circ$ to the a axis of the crystal and the magnetic moment along this axis was $m = (m_a^2 + m_b^2)^{1/2} = 8.7\mu_B$.

The magnetization and torque curves recorded at different temperatures were used to plot the temperature dependence of the spontaneous magnetization (Fig. 2a). It is clear from Fig. 2a that at a temperature above 60 K the spontaneous magnetic moment is oriented along the c axis [with the $\Gamma_4(G_x F_z)$ magnetic structure] and cooling increased the magnetic moment along the c axis strongly in a temperature interval $\Delta T \approx 1$ K and then the magnetization "tail" along the c axis extended right up to 52 K. It should be pointed out that in the temperature range of a steep fall of the

magnetization, i.e., at $T_1 = 60 \pm 1$ K, there was a maximum of the susceptibility along the c axis (Fig. 1b). Hence, a spin reorientation occurred near this temperature and the magnetization tail was clearly associated with an inhomogeneity of the sample.

In this temperature range a magnetic moment appeared along the a axis; this moment first increased strongly as a result of cooling, reaching its maximum value of $m_x^0 = 2.1 \text{ G} \cdot \text{cm}^3 \cdot \text{g}^{-1}$ at 59 K, and then fell; the fall of the magnetization along the a axis was steep down to 57 ± 1 K and then the rate of fall slowed down stopping completely at 52 K. Below 8 K the spontaneous magnetic moment reappeared along the a axis (Fig. 2a) and rose hyperbolically as a result of cooling. We identified the magnetic structure of $\text{HoFe}_{0.97}\text{Al}_{0.03}\text{O}_3$ that gave rise to the magnetic moment along the a axis by comparing the value of this moment with the induced moment in the $\Gamma_2(G_z F_x)$ phase (Fig. 2a), which was found by extrapolating to zero field of the magnetization curves along the a axis recorded in magnetic fields exceeding the threshold field for the transition to the $\Gamma_2(G_z F_x)$ phase.

A comparison of the spontaneous m_x^0 and induced m_x^{ind} moments (Fig. 2a) showed that at all temperatures the inequality $m_x^0 < m_x^{\text{ind}}$ was obeyed and, consequently, the structure was not the $\Gamma_2(G_z F_x)$ magnetic structure, but a canted

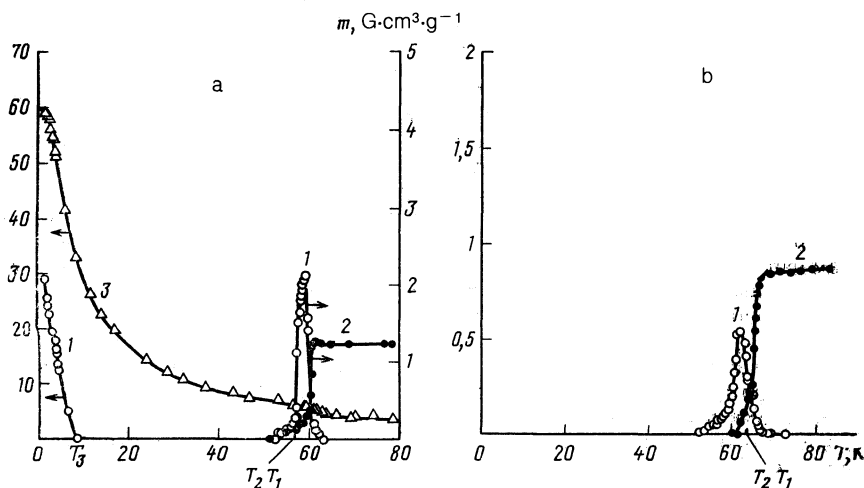


FIG. 2. Temperature dependences of the spontaneous (m_x^0 and m_y^0 are represented by curves 1 and 2) and induced (m_x^{ind} , curve 3) weak ferromagnetic moments of $\text{HoFe}_{0.97}\text{Al}_{0.03}\text{O}_3$ (a) and $\text{HoFe}_{0.93}\text{Al}_{0.07}\text{O}_3$ (b). The pointers on the abscissa identify $T_2 = 57$ K in Fig. 2a and $T_1 = 65$ K in Fig. 2b (see text).

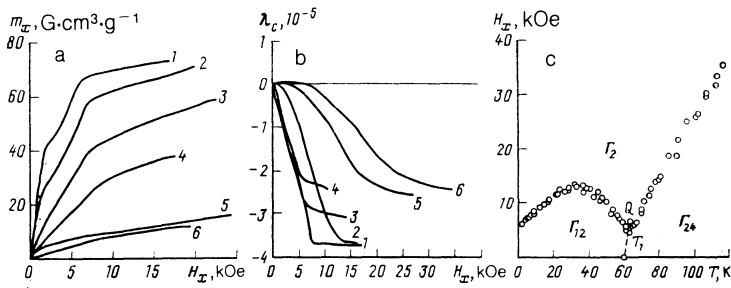


FIG. 3. Magnetization curves (a), magnetostriction isotherms along the c axis (b), and H - T phase diagram (c) of $\text{HoFe}_{0.93}\text{Al}_{0.07}\text{O}_3$ in fields $\mathbf{H}\parallel\mathbf{a}$. a: 1) 1.6 K; 2) 4.2 K; 3) 8.7 K; 4) 17 K; 5) 60.7 K; 6) 78 K. b: 1) 4.7 K; 2) 45.5 K; 3) 59 K; 4) 61.5 K; 5) 86.4 K; 6) 103 K. c: Q is the bicritical point.

structure of the $\Gamma_{12}(G_z G_y F_x)$ type. The appearance of a magnetic moment along the a axis at $T_3 = 8$ K indicated the occurrence of the $\Gamma_1 \rightarrow \Gamma_{12}$ orientational transition at this temperature. At higher temperatures there were clearly two unusual, for orthoferrites, reorientational transitions $\Gamma_4 \rightarrow \Gamma_{12}$ ($T_1 = 60 \pm 1$ K) and $\Gamma_{12} \rightarrow \Gamma_1$ ($T_2 = 57 \pm 1$ K), which were close on the temperature scale.¹⁾ Since, in contrast to HoFeO_3 , the $\Gamma_4 \rightarrow \Gamma_{24}$ reorientational transition did not occur in $\text{Ho}_{0.97}\text{Fe}_{0.03}\text{AlO}_3$ and the low-temperature phase $\Gamma_2(G_z F_x)$ did not appear in this compound, and since the reorientational transitions $\Gamma_4 \rightarrow \Gamma_{12}$ and $\Gamma_{12} \rightarrow \Gamma_1$ were close on the temperature scale, we concluded that major changes in the anisotropy constants occurred under the influence of the magnetic vacancies, and that these changes suppressed the Γ_2 magnetic structure and stabilized the antiferromagnetic Γ_1 structure.

Major changes in the magnetic anisotropy when the nonmagnetic Al^{3+} ions are introduced were observed also for the composition with $x = 0.07$ (Fig. 2b), in which at temperatures $T_1 = 65 \pm 1$ K and $T_2 = 60 \pm 1$ K there were reorientational transitions similar to those occurring in the composition with $x = 0.03$. An even greater spread of the transition along the temperature scale (compared with that in the sample with $x = 0.03$) observed in this case was clearly due to a greater inhomogeneity of the sample. As this composition cooled further, in contrast to the sample with $x = 0.03$, the antiferromagnetic $\Gamma_1(G_y)$ structure was observed at all temperatures and this was clearly due to an increase in the contribution made to the anisotropy by the magnetic vacancy mechanism which stabilized the $\Gamma_1(G_y)$ phase.

In addition to the spontaneous reorientational transitions in the investigated orthoferrites containing the Al^{3+} impurity ions, there were also external-magnetic-field induced spin-reorientation transitions in fields $\mathbf{H}\parallel\mathbf{a}$, $\mathbf{H}\parallel\mathbf{b}$, $\mathbf{H}\parallel\mathbf{c}$. The application of a magnetic field with the $\mathbf{H}\parallel\mathbf{a}$ orientation gave rise to the $\Gamma_{24} \rightarrow \Gamma_2$ and $\Gamma_{12} \rightarrow \Gamma_2$ transitions in a fairly high magnetic field H' whose value was determined in the usual way from the bend in the field dependence of the magnetization (Fig. 3a)²⁾ and from the magnetostriction (Fig. 3b).³⁾ It is clear from Fig. 3a that the nature of the magnetization isotherms changed as the temperature increased. The low-temperature curves 1 and 2 corresponding to $T = 1.6$ and 4.2 K clearly revealed magnetization jumps typical of the first-order phase transitions, whereas the curves recorded at $T = 8.7$ K or higher temperatures did not show these jumps. The experimentally determined tricritical point was $T_{ic} \approx 8$ K. Similar anomalies were reported in Refs. 4 and 5 and were explained by a strong magnetization

reversal of the rare-earth ions whose environment included magnetic vacancies. It is clear from Fig. 3b that the magnetostriction which appeared as a result of the $\Gamma_{12} \rightarrow \Gamma_2$ transition at low temperatures amounted to $\lambda_c = -(3.7 \pm 0.3) \cdot 10^{-5}$, whereas above 60 K, where the field induced the orientational $\Gamma_{24} \rightarrow \Gamma_2$ transition, the magnetostriction fell in the sense of the absolute value to $\lambda_c = -(2.3 \pm 0.2) \cdot 10^{-5}$ and remained constant at higher temperatures.

Figure 3c shows the corresponding experimental H_x - T phase diagram obtained for the $\text{HoFe}_{0.97}\text{Al}_{0.03}\text{O}_3$ composition. It is clear from Fig. 3c that the threshold field for inducing the reorientation to the Γ_2 phase was minimal (~ 5 kOe) near the spontaneous $\Gamma_4 \rightarrow \Gamma_{12}$ reorientation temperature; it rose monotonically away from the range of temperatures where the spontaneous spin reorientation was observed. Cooling first increased the threshold field which induced the $\Gamma_{12} \rightarrow \Gamma_2$ transitions and this field passed through a maximum and fell again, reaching the value ~ 6 kOe at 1.8 K. The low-temperature fall of the threshold field was not caused by the approach to the $\Gamma_1 \rightarrow \Gamma_{12}$ spin reorientation temperature, but was due to the effects of the magnetic-field-enhancement of the molecular field exerted on the iron subsystem by the rare-earth ions as observed earlier,^{3,10} and this effect became stronger as a result of cooling.

In a field $\mathbf{H}\parallel\mathbf{c}$ the reorientation to the Γ_4 phase accompanied by the appearance of the magnetostriction was induced in fields up to 40 kOe only in a temperature interval ~ 10 K close to the high-temperature spontaneous spin reorientations (Fig. 4a). At temperatures $T > 62$ K and $T < 50$ K the magnetostriction was due to the paramagnetism of the rare-earth ions and was a quadratic function of the field. Cooling in the range $52 \text{ K} < T < 61 \text{ K}$ gave rise to negative jumps of the magnetostriction superposed on the paramagnetic contribution: these jumps corresponded to the reorientation of the spins from the canted Γ_{124} phase to the Γ_4 phase, which was clearly a first-order phase transition. A first-order reorientational transition is known¹¹ to occur usually via an intermediate state representing the coexistence of both phases, giving rise to some spread of the transition in a finite interval of the fields. Bearing this point in mind, we concluded that the threshold in this case was the field at which the Γ_4 phase just appeared, i.e., the field of the onset of the magnetostriction jump. The corresponding H_x - T phase diagram (Fig. 4b) shows the interval of fields where the intermediate state was observed. Clearly, the threshold field inducing the $\Gamma_{124} \rightarrow \Gamma_4$ reorientation rose rapidly as a result of cooling, so that at 50 K the magnetic fields available to us in the experimental setup were too weak

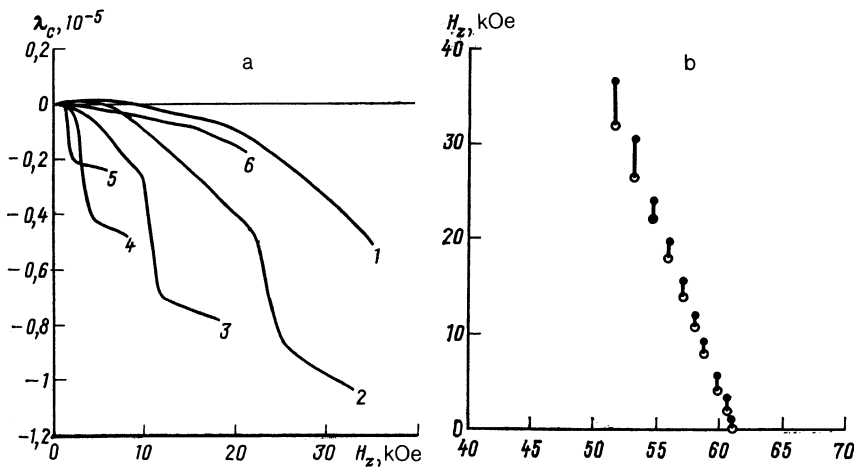


FIG. 4. Magnetostriction isotherms (a) and H - T phase diagram (b) of $\text{HoFe}_{0.97}\text{Al}_{0.03}\text{O}_3$ in fields $\mathbf{H}\parallel\mathbf{c}$. a: 1) 44 K; 2) 54.5 K; 3) 58 K; 4) 60.6 K; 5) 61.5 K; 6) 62 K.

to complete the induced spin reorientation.

In the case of $\text{HoFe}_{0.93}\text{Al}_{0.07}\text{O}_3$ the H_x - T and H_z - T phase diagrams were similar (Figs. 5a and 5b).

Interesting external-field-induced reorientations occurred in $\text{HoFe}_{0.93}\text{Al}_{0.07}\text{O}_3$ when the field was $\mathbf{H}\parallel\mathbf{b}$. The field dependences of the magnetostriction (Fig. 6a) were unusual at low temperatures and exhibited two negative jumps against the background of a rising positive magnetostriction, which was due to the rare-earth ions. Clearly, these anomalies were associated with the processes of reversal of the magnetization of the Ho^{3+} ions, accompanied by spin reorientation in the Fe subsystem. The application of a field along the \mathbf{b} axis, which was the antiferromagnetic axis at low temperatures, facilitated a reorientation of the spin-flop type and made possible transitions from the $\Gamma_{23}(G_y)$ antiferromagnetic state either to the $\Gamma_{34}(G_x)$ or the $\Gamma_{23}(G_z)$ phase. Bearing in mind that in the case of pure HoFeO_3 (Ref. 12) a field $\mathbf{H}\parallel\mathbf{b}$ of ~ 20 – 40 kOe intensity induced the $\Gamma_{34}(G_x)$ phase and suppressed $\Gamma_{23}(G_z)$, we concluded that in our case the final phase in this geometry was also $\Gamma_{34}(G_x)$. Therefore, an increase in the field $\mathbf{H}\parallel\mathbf{b}$ in $\text{HoFe}_{0.93}\text{Al}_{0.07}\text{O}_3$ resulted in $\Gamma_{13}(G_y) - \Gamma_{34}(G_x)$, spin reorientation. This occurred in two stages clearly involving an intermediate phase

due to the successive magnetization reversal of the Ho^{3+} ions located at inequivalent positions. It should be pointed out that the existence of an intermediate ($G_{x,y,z}$) phase, and not of the collinear $\Gamma_{23}(G_z)$ phase, was confirmed by the observation that in the case of the $\Gamma_{13}(G_y) - \Gamma_{23}(G_z)$ transition the magnetostriction anomaly would have been positive and much larger ($\sim 4 \times 10^{-5}$).³

In the case of the composition $\text{HoFe}_{0.97}\text{Al}_{0.03}\text{O}_3$ the reorientations in strong fields were qualitatively similar, but in lower fields the low-temperature magnetostriction curves had an additional anomaly which was clearly associated with the $\Gamma_{123} \rightarrow \Gamma_{13}$ transition, as shown in Fig. 6b (this point is discussed below).

THEORY AND DISCUSSION OF RESULTS

Our interpretation of the spontaneous and field-induced phase transitions in $\text{HoFe}_{1-x}\text{Al}_x\text{O}_3$ will be based on a model in which the Ho^{3+} ions are considered in the one-doublet approximation. The influence of the excited states of the Ho^{3+} ions of $E \gg 100$ K energy, which also play an important role in the magnetic properties of the system,^{6,7} will be allowed for by renormalization of the relevant coefficients of the thermodynamic potential of the Fe subsystem. The

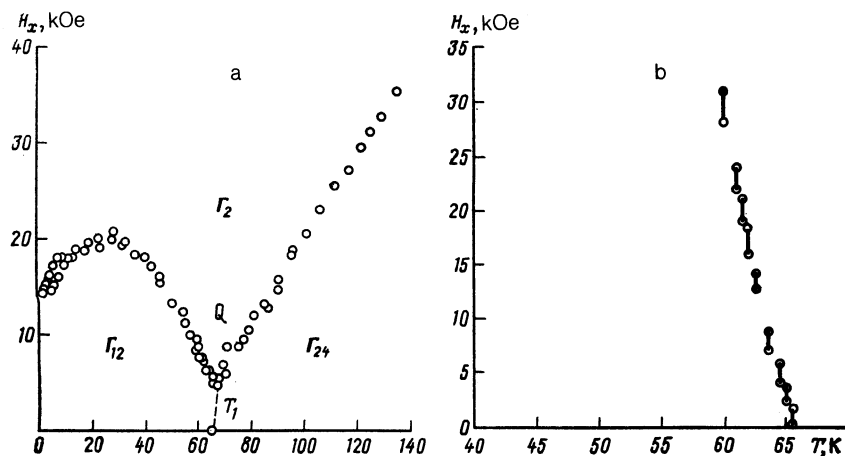


FIG. 5. Phase (H - T) diagrams of $\text{HoFe}_{0.93}\text{Al}_{0.07}\text{O}_3$ in fields $\mathbf{H}\parallel\mathbf{a}$ (a) and $\mathbf{H}\parallel\mathbf{c}$ (b).

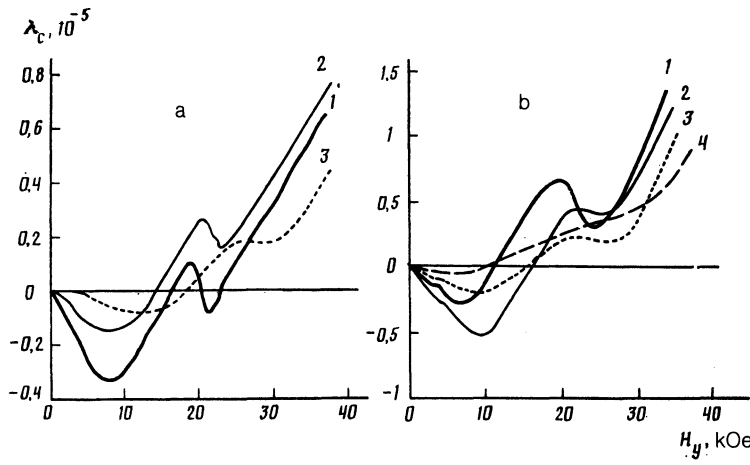


FIG. 6. Magnetostriction isotherms along the c axis obtained in $\mathbf{H} \parallel \mathbf{b}$ fields for $\text{HoFe}_{0.97}\text{Al}_{0.03}\text{O}_3$ (a) and $\text{HoFe}_{0.93}\text{Al}_{0.07}\text{O}_3$ (b). a: 1) 2.4 K; 2) 3.52 K; 3) 5.4 K. b: 1) 2.63 K; 2) 4.2 K; 3) 5.9 K; 4) 8.1 K.

order parameters of the Ho subsystem are the average values of the Pauli matrices of the quasidoublets of the Ho^{3+} ions

$$\langle \hat{\sigma}_i \rangle \equiv \hat{\sigma}_i \equiv (\hat{\sigma}_{iz}, \hat{\sigma}_{iy}, \hat{\sigma}_{ix}),$$

which are in an effective field created by the f - d and f - f interactions and in an external magnetic field \mathbf{H} . The state of the d subsystem is described, as usual, by the dimensionless ferromagnetic and antiferromagnetic vectors (\mathbf{F}, \mathbf{G}) . The nonequilibrium thermodynamic potential of the system per molecule of $\text{HoFe}_{1-x}\text{Al}_x\text{O}_3$ can be represented, by analogy with Refs. 6 and 13, in the form

$$\Phi(\mathbf{F}, \mathbf{G}, \sigma_i, \sigma'_j)$$

$$= \tilde{\Phi}_{\text{Fe}}(\mathbf{F}, \mathbf{G}) - \frac{1}{2}(1-zx) \sum_{i=1}^2 \sigma_i \mathbf{h}_i - \frac{1}{4}zx \sum_{j=1}^4 \sigma'_j \mathbf{h}'_j - \frac{1}{2}\lambda_f \mathbf{F}^2 - \frac{1}{2}\lambda_c \bar{c}^2 - \frac{1}{2}(1-zx)T \times \sum_{i=1}^2 S(|\sigma_i|) - \frac{1}{4}zxT \sum_{j=1}^4 S(|\sigma'_j|), \quad (1)$$

where

$$\tilde{\Phi}_{\text{Fe}}(\mathbf{F}, \mathbf{G}) = \frac{1}{2}A\mathbf{F}^2 - d(\mathbf{F}_x\mathbf{G}_z - \mathbf{F}_z\mathbf{G}_x) - \tau_1 H_x G_z - \tau_3 H_z G_x - \mu_{\text{Fe}} \mathbf{F} \mathbf{H} + \Phi_A(\mathbf{G}), \quad (2)$$

$$\Phi_A(\mathbf{G}) = \frac{1}{2}K_{ac} G_z^2 + \frac{1}{2}K_{ab} G_y^2 + \frac{1}{4}K_2 G_z^4 + \frac{1}{4}K_2' G_y^4 + \frac{1}{2}K_2'' G_y^2 G_z^2. \quad (3)$$

Here, $\tilde{\Phi}_{\text{Fe}}$ are the thermodynamic potentials of the Fe subsystem renormalized by the Van Vleck contribution of the excited states of the Ho^{3+} ions, depending weakly on temperature in the range $T < 100$ K. The other terms in Eq. (1) represent the contribution made to the thermodynamic potential by the ground quasidoublet of the Ho^{3+} ions. The quantities σ'_j ($j = 1-4$) and σ_i ($i = 1, 2$) are the average values of the Pauli matrices of the Ho^{3+} ions which, respectively, have one vacancy in their environment within the Fe subsystem (i.e., the Al^{3+} ions), and no such a vacancy, whereas \mathbf{h}'_j and \mathbf{h}_i represent the corresponding effective fields whose

moduli are equal to the half-splitting of the ground quasidoublet of the Ho^{3+} ion:

$$\mathbf{h}'_j = (\Delta_{0v} + (\mu_v \mathbf{H}_{MB}^{(n)}), 0, \Delta_{\text{qd}}), \quad (4a)$$

$$\mathbf{h}_i = (\Delta_{0v}, 0, \Delta_{\text{qd}}), \quad (4b)$$

where

$$\Delta_{0v} = \Delta_{\text{ex}} G_z + (\mu_v(\mathbf{H} + a\mathbf{F})) + \lambda_f \bar{f} + \nu \lambda_c \bar{c}, \quad (5)$$

where Δ_{qd} is the half-splitting of the ground quasidoublet of the Ho^{3+} ion in a crystal field (amounting to $\Delta_{\text{qd}} \approx 2.3$ K, according to Ref. 3); a and Δ_{ex}^0 are constants of, respectively, the isotropic and anisotropic f - d exchange interactions; $\mu_v = (\mu_x, \nu \mu_y, 0)$ is the magnetic moment of the quasidoublet of the Ho^{3+} ion along the Ising axis lying in the \mathbf{ab} plane of the crystal at an angle $\alpha = \tan^{-1}(\nu \mu_y / \mu_x) = 65^\circ$ to the \mathbf{a} axis; $|\mu_v| = \mu_0$, $\lambda_{f,c}$ are the constants of the f - f interaction; the quantities

$$\bar{f}, \bar{c} = \frac{1}{2}(1-zx)(\sigma_1 \pm \sigma_2) + \frac{1}{4}zx(\sigma'_1 + \sigma'_2 \pm \sigma'_3 \pm \sigma'_4), \quad (6)$$

where the plus sign corresponds to \mathbf{f} and the minus sign corresponds to \bar{c} , whereas the components \bar{f}_ξ and \bar{c}_ξ govern the contribution made to the magnetization of the Ho subsystem along the \mathbf{a} and \mathbf{b} crystal axes;

$$\mathbf{H}_{\text{mv}}^{(\eta)} = \eta H_{\text{mv}} \mathbf{G} \quad (7)$$

is the field of a magnetic vacancy at an Ho^{3+} ion due to decompensation of its antiferromagnetic d environment ($H_{\text{mv}} \approx 10^4$ Oe);

$$S(y) = \ln 2 - \frac{1}{2}(1+y) \ln(1+y) - \frac{1}{2}(1-y) \ln(1-y),$$

is the entropy of a two-level system. In Eqs. (4)-(5) and (7) the quantity $\nu = \pm 1$ distinguishes two crystallographically inequivalent positions of the Ho^{3+} ions, whereas the quantity $\eta = \pm 1$ identifies the type of the site occupied by a magnetic vacancy. Therefore, the number of inequivalent positions of the Ho^{3+} ions with one magnetic vacancy in their immediate environment is four: $j = 1$ corresponds to $\nu = 1$, $\eta = 1$; the other sets are $j = 2 - \nu = 1$, $\eta = -1$; $j = 3 - \nu = -1$, $\eta = 1$ and $j = 4 - \nu = -1$, $\eta = -1$; in the case of those ions which have no vacancies in their vicinity the number of inequivalent positions reduces to two. In deriving the thermodynamic potentials of Eq. (1) the con-

centration x of the magnetic vacancies is assumed to be low and it is postulated that no more than one vacancy is located in the immediate environment of an Ho^{3+} ion. Minimization of the thermodynamic potential of Eq. (1) with respect to \mathbf{F} allowing for $\mathbf{F} \cdot \mathbf{G} = 0$, $G^2 = 1 - F^2 \approx 1$, and eliminating from Eq. (1)

$$\mathbf{F} = \chi_{\perp} [\mathbf{H}_i - (\mathbf{H}_i \mathbf{G}) \mathbf{G}] / \mu_{\text{Fe}},$$

reduces the thermodynamic potential to

$$\begin{aligned} \Phi(\mathbf{G}, \boldsymbol{\sigma}_i, \boldsymbol{\sigma}'_j) = & \Phi_A(\mathbf{G}) - \tau_1 H_x G_x - \tau_3 H_z G_z - \frac{1}{2} \chi_{\perp} [\mathbf{H}_i^2 - (\mathbf{H}_i \mathbf{G})^2] \\ & - (\mu_x H_x + \Delta_{ex} G_x) \bar{f}_{\xi} - \mu_y H_y \bar{c}_{\xi} - z x (\Delta_x G_x g_{\xi}' + \Delta_y G_y a_{\xi}') - \frac{1}{2} \lambda_f \bar{f}_{\xi}^2 \\ & - \frac{1}{2} \lambda_c \bar{c}_{\xi}^2 - \Delta_{qd} \bar{f}_{\xi} - \frac{1}{2} (1 - z x) T \sum_{i=1}^2 S(|\boldsymbol{\sigma}_i|) - \frac{1}{4} z x T \sum_{j=1}^4 S(|\boldsymbol{\sigma}_j|), \end{aligned} \quad (8)$$

where

$$\begin{aligned} g_{\xi}' = & \frac{1}{4} (\sigma_{\xi 1}' - \sigma_{\xi 2}' + \sigma_{\xi 3}' - \sigma_{\xi 4}'), \quad a_{\xi}' = \frac{1}{4} (\sigma_{\xi 1}' - \sigma_{\xi 2}' - \sigma_{\xi 3}' + \sigma_{\xi 4}'), \\ \mathbf{H}_i = & (H_x + H_D G_x + \bar{\mu}_x a \bar{f}_{\xi}, H_y + \bar{\mu}_y a \bar{c}_{\xi}, H_z - H_D G_z), \quad (9) \\ \chi_{\perp} = & \mu_{\text{Fe}} / A, \quad H_D = d / \mu_{\text{Fe}}, \quad \bar{\mu}_{x,y} = \mu_{x,y} / \mu_{\text{Fe}}, \\ \Delta_x = & \Delta_{mv} \cos \alpha, \quad \Delta_y = \Delta_{mv} \sin \alpha, \quad \Delta_{MB} = \mu_0 H_{mv}. \end{aligned}$$

We use Eq. (8) to analyze the phase transitions in $\text{HoFe}_{1-x}\text{Al}_x\text{O}_3$. We shall begin with the spontaneous reorientations. Since they occur at fairly high temperatures ($T > |\mathbf{h}_i|$), we can consider them by confining ourselves to the high-temperature approximation when $|\boldsymbol{\sigma}_j| \ll 1$. In this case if we expand $S(|\boldsymbol{\sigma}_j|)$, minimize the thermodynamic potentials of Eq. (8) with respect to $\boldsymbol{\sigma}_i$ and $\boldsymbol{\sigma}'_j$, and eliminate them from this expression, we still have the same standard form (see Refs. 3, 6, 7, and 13) which is a function of $\mathbf{G} = (\sin \theta \sin \varphi, \sin \theta \cos \varphi, \cos \theta)$ alone, but the coefficients are renormalized. For $H = 0$ the thermodynamic potential reduces to the anisotropy energy $\Phi_A(\mathbf{G})$ in the form of Eq. (3), where

$$\begin{aligned} K_{ac} = & K_{ac}^0 - \frac{\Delta_{ex}^2}{T + \theta_x} + \frac{z x (\Delta_{mv} \cos \alpha)^2}{T}, \\ K_{ab} = & K_{ab}^0 + \frac{z x \Delta_{mv}^2 \cos 2\alpha}{T}, \end{aligned} \quad (10)$$

where

$$\Delta_{ex} = \Delta_{ex}^0 + ad/A, \quad K_{ab}^0 = K_{ab}^{0'} + d^2/A, \quad \theta_{x,y} = -\lambda_{f,c}$$

are the paramagnetic temperatures along the x (\mathbf{a}) and y (\mathbf{b}) crystal axes, respectively. It is clear from Eq. (10) that the magnetic vacancies make a contribution (which increases as a result of cooling) to the anisotropy constants in the \mathbf{ac} plane (K_{ac}) and in the \mathbf{ab} plane (K_{ab}). In the \mathbf{ac} plane this contribution is positive and it stabilizes the $\Gamma_4(G_x F_x)$ phase, whereas, in the \mathbf{ab} plane it is negative (because $\cos 2\alpha < 0$) and it stabilizes the $\Gamma_1(G_y)$ phase. On the other hand, K_{ac} includes also a negative contribution associated with the exchange splitting in the $\Gamma_2(G_z F_x)$ phase, which stabilizes the latter and thus competes with the magnetic vacancy contribution. It should be pointed out also that pure holmium orthoferrite exhibits, in the region of the spontaneous spin reorientation, a reduction in the constant K_{ab}^0 as a result of cooling and reversal of the sign (at $T \sim 50$ K) because of the negative van Vleck contribution; then for $T \leq 30$ K this constant reaches saturation.⁶

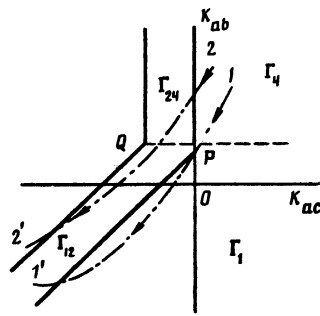


FIG. 7. Phase diagram of orthoferrites in the space of the two anisotropy constants K_{ac} and K_{ab} . Here, lines 1-1' and 2-2' represent the schematic thermodynamic path of the $\text{HoFe}_{0.97}\text{Al}_{0.03}\text{O}_3$ composition and of pure HoFeO_3 , respectively.

The equilibrium configurations of the investigated system and the spontaneous transitions between these configurations can be illustrated conveniently in a phase diagram plotted in the space of the effective anisotropy constants K_{ac} and K_{ab} . Since the fourth-order anisotropy constants of orthoferrites, governed at high temperatures mainly by the Fe subsystem, satisfy the inequalities $K_2 > 0$, $K_2 < 0$, and $\bar{K}_2 = K_2' + K_2 - 2K_2'' > 0$, this phase diagram has the form shown in Fig. 7 (Ref. 6). An important feature of the diagram is the presence (in the range $K_2' > 2K_2''$) of a first-order phase transition line separating the Γ_4 and Γ_{12} phases, which makes it possible to account for the abrupt $\Gamma_4 \rightarrow \Gamma_{12}$ transition observed at $T_1 = 60$ K. On the whole, the $\Gamma_4 \rightarrow \Gamma_{12} \rightarrow \Gamma_1 \rightarrow \Gamma_{12}$ phase transitions observed in $\text{HoFe}_{1-x}\text{Al}_x\text{O}_3$ ($x = 0.03$) correspond to the passage of the system along the thermodynamic path 1-1' (Fig. 7), which exhibits—at T_1 —a jump of the vector \mathbf{G} from the \mathbf{a} axis (Γ_4 phase) to the canted orientation (Γ_{12}), then at T_2 it rotates smoothly to the \mathbf{b} axis (Γ_1), and finally at T_3 it deviates smoothly from the \mathbf{b} axis to the \mathbf{bc} plane (Γ_{12}).

For comparison, we included in the $K_{ac}-K_{ab}$ phase diagram also a thermodynamic path 2-2' of pure holmium orthoferrite representing the $\Gamma_4 \rightarrow \Gamma_{24} \rightarrow \Gamma_{12} \rightarrow \Gamma_2$ phase transitions. According to Eq. (10), a change in the thermodynamic path of $\text{HoFe}_{1-x}\text{Al}_x\text{O}_3$ compared with HoFeO_3 is due to the negative contribution of the magnetic vacancies to the anisotropy constant in the \mathbf{ab} plane (K_{ab}), which stabilizes the Γ_1 phase, and a positive contribution to K_{ac} , which stabilizes the Γ_4 phase. However, the latter competes with the negative contribution to the K_{ac} associated with the exchange splitting Δ_{ex} of the Ho^{3+} doublet in the $\Gamma_2(G_z F_x)$ phase, which maintains the tendency for the \mathbf{G} vector to tilt out of the \mathbf{ab} plane.

We now consider in greater detail the conditions under which the phase transitions take place. Along the phase transition line between the Γ_4 phase and the canted phase Γ_{12} , which is characterized by

$$G_{z0}^2 = \cos^2 \theta_0 = -K_{bc} / \bar{K}_2, \quad (11)$$

we find equating the corresponding thermodynamic potentials yields

$$K_{ab} + \frac{1}{2} K_2' = \frac{1}{2} K_{bc}^2 / \bar{K}_2, \quad (12)$$

where

$$K_{bc} = K_{ac} - K_{ab} - K_2' + K_2'' < 0, \quad \bar{K}_2 = K_2 + K_2' - 2K_2'' > 0$$

are the effective second- and fourth-order anisotropy constants which apply in the bc plane. Near the Γ_{4-12} phase transition the experimental value of the spontaneous magnetic moment is $m_x^0 = m_x G_{20} \sim 2 \text{ G} \cdot \text{cm}^3 \cdot \text{g}^{-1}$ for the Γ_{12} phase and the magnetic moment induced by the $\mathbf{H} \parallel \mathbf{a}$ field is $m_x^{\text{ind}} = m_x \sim 6 \text{ G} \cdot \text{cm}^3 \cdot \text{g}^{-1}$ for the Γ_2 phase, so that the angle is $\theta_0 \approx 70^\circ$. The $\Gamma_{12} - \Gamma_1$ phase transition line is deduced from the condition $K_{bc}(T_2) = 0$, which imposes the restraint $\Delta_{ex}^2 < zx \Delta_{mv}^2 \sin^2 \alpha$.

The high-temperature approximation of Eq. (10) is insufficient to account for the reverse $\Gamma_1 - \Gamma_{12}$ phase transition at a lower temperature T_3 and we have to use the initial thermodynamic potential of Eq. (8). In this case the stability of the Γ_1 phase in the bc plane is characterized by the quantity

$$\left(\frac{\partial^2 \Phi}{\partial \theta^2} \right)_{\Gamma_1} = \left(\frac{\partial^2 \Phi}{\partial \theta^2} \right)_{\Gamma_1} + \sum \frac{\partial^2 \Phi}{\partial \theta \partial X_k} \frac{\partial X_k}{\partial \theta} = K_{bc} = K_{bc}^0 - (1-zx) (\Delta_{ex}^2 / \Delta_{qd}) \text{th}(\Delta_{qd}/T) + zx \{ \Delta_y^2 / \Delta_1 \text{th}(\Delta_1/T) - \Delta_{ex}^2 [(\Delta_{qd}^2 / \Delta_1^3) \text{th}(\Delta_1/T) + \Delta_y^2 / (\Delta_1 T \text{ch}^2(\Delta_1/T))] \}, \quad (13)$$

where X_k are the variables of the f subsystem, and

$$K_{bc}^0 = K_{ac}^0 - K_{ab}^0 - K_2' + K_2'', \quad \Delta_1^2 = \Delta_{qd}^2 + \Delta_y^2.$$

Equation (13) is derived ignoring, for the sake of simplicity, the $R-R$ interaction. At high temperatures ($T \gg \Delta_1$) we have $\bar{K}_{bc} \rightarrow K_{bc}$. At low temperatures the value of \bar{K}_{bc} changes sign and the Γ_1 phase becomes unstable because of an increase in the negative contribution of the second term in Eq. (13), which is due to the same Ho^{3+} ions whose environment does not include any magnetic vacancies. For $\Delta_{qd} \approx 0$ there is a divergence at low values of T . This reflects the fact that in a system containing ions with a degenerate (or near degenerate) ground state (which is true of the Ho^{3+} ions without any nearby magnetic vacancies in the Γ_1 phase), an instability appears and tends to lift this degeneracy (magnetic analog of the Jahn-Teller effect¹³). In the present case this instability appears as the $\Gamma_1 \rightarrow \Gamma_{12}$ phase transition back to the canted phase when $\bar{K}_{bc}(T_3) = 0$. Our experimental results indicate that this canted phase exists in the sample with $x = 0.03$ right down to $T = 0 \text{ K}$. An increase in the magnetic vacancy concentration weakens this mechanism, as expected on the basis of Eq. (13). This is clearly true of our $x = 0.07$ sample, which right down to $T \sim 2 \text{ K}$ did not exhibit a reverse transition to the Γ_{12} canted phase.

We now consider the magnetic structure of the d and f subsystems at $T = 0 \text{ K}$. In this case the projections of the equilibrium magnetic moments of the Ho^{3+} ions onto the corresponding Ising axis are (for $\Delta_{ex} \gg \Delta_{mv}$ and $\Delta_{ex} \gg \Delta_{qd}$)

$$\mu_j' = \mu_0 \text{sign}(h_{\xi j}'), \quad j=1-4; \\ \mu_i = \mu_0 \text{sign}(h_{\xi i}), \quad i=1-2, \quad (14)$$

for the ions which have and do not have a magnetic vacancy in their environment; the components $h_{\xi j}'$ and $h_{\xi i}$ of the effective fields are given by Eqs. (4a) and (4b), respectively. Bearing in mind that in the case of HoFeO_3 we have

$$\Delta_{ex}, \Delta_{mv} \gg |K_{ac}|, |K_{ab}|, |K_2|, |K_2'|, |K_2''|, (\mu_0 a)^2 / \Delta$$

we can at low temperatures and for $H \leq 5 \cdot 10^4 \text{ Oe}$ simplify the thermodynamic potential of Eq. (8) by dropping the first four terms. Consequently, the orientation of the vector \mathbf{G} will then be governed by just its interaction ($-\mathbf{G} \cdot \mathbf{h}_G$) with the effective field $\mathbf{h}_G = (zx \Delta_x g_{\xi}', zx \Delta_y \alpha_{\xi}', \Delta_{ex} \bar{f}_{\xi})$ exerted by the Ho subsystem and not dependent explicitly on the external field \mathbf{H} . This means that the external field influences the Fe subsystem mainly indirectly via the Ho subsystem. An analysis of the equilibrium properties on the basis of Eqs. (8) and (14) shows that for $H = 0$, we can have three magnetic configurations in which the Fe subsystem is in the states $\Gamma_2(G_z F_z)$, $\Gamma_{12}(G_{y,z} F_x)$, and $\Gamma_1(G_y)$, respectively.

If the value of Δ_{mv} is small, we can expect—as in the case of pure HoFeO_3 —the A' phase for which the vector \mathbf{G} is oriented along the c axis [$\Gamma_2(G_z F_z)$ phase], whereas the Ho subsystem has the strongest magnetization along the a axis. The phase in question is doubly degenerate:

- a) $G_z = 1, \quad \mu_{1,2} = \mu_{1,2,3,4} = \mu_0,$
- b) $G_z = -1, \quad \mu_{1,2} = \mu_{1,2,3,4} = -\mu_0.$

As Δ_{mv} increases, if $\Delta_0 > \Delta_{ex} - \theta_x zx (1 - \frac{1}{2} zx)$, where

$$\Delta_0 = [(1-zx)^2 \Delta_{ex}^2 + (zx \Delta_y)^2]^{1/2}$$

the A phase with the Fe subsystem characterized by the canted configuration Γ_{12} is preferred and the magnetic structure of those Ho^{3+} ions which have magnetic vacancies in their environment represents a "cross" formed by the magnetic moments of the Ho^{3+} ions with different orientations (Fig. 8a). However, the ions which have no vacancies in their vicinity are magnetized along the corresponding Ising axis by the exchange field ($\Delta_{ex} G_z$). This magnetic configuration (phase A in Fig. 8a) is quadruply degenerate and is characterized by the following variables:

- a) $\mu_{1,4}' = \mu_0, \quad \mu_{2,3}' = -\mu_0, \quad \mu_{1,2} = \mu_0, \quad \theta = \theta_0, \quad \varphi = \pi/2,$
- b) $\mu_{1,4}' = \mu_0, \quad \mu_{2,3}' = -\mu_0, \quad \mu_{1,2} = -\mu_0, \quad \theta = \pi - \theta_0, \quad \varphi = \pi/2,$
- c) $\mu_{1,4}' = -\mu_0, \quad \mu_{2,3}' = \mu_0, \quad \mu_{1,2} = \mu_0, \quad \theta = \theta_0, \quad \varphi = -\pi/2,$
- d) $\mu_{1,4}' = -\mu_0, \quad \mu_{2,3}' = \mu_0, \quad \mu_{1,2} = -\mu_0, \quad \theta = \pi - \theta_0, \quad \varphi = -\pi/2.$

The positive directions of the magnetic moments along the Ising axes correspond to μ_1' and μ_4' in Fig. 8a. The angle θ_0 governing the orientation \mathbf{G} relative to the c axis in the bc plane (Γ_{12}) is found by minimization of the thermodynamic potential of Eq. (8) and is given by

$$\sin \theta_0 = zx \Delta_y / \Delta_0. \quad (15)$$

When the value of Δ_{mv} is even greater [$2zx \Delta_y \Delta_{qd} \gg \Delta_{ex}^2 (1 - zx)$], the magnetic configuration (phase B) has the Fe subsystem in the state $\Gamma_1(G_y)$ and the magnetic structure of the Ho^{3+} ions with magnetic vacancies in their vicinity is again a cross. The remaining Ho^{3+} ions are not magnetized, because the splitting of their ground state is governed solely by Δ_{qd} . This configuration is doubly degenerate and is characterized by the following values of the variables: $G_y = 1, \mu_{1,4}' = \mu_0, \mu_{2,3}' = -\mu_0; G_y = -1, \mu_{1,4}' = -\mu_0, \mu_{2,3}' = \mu_0$.

Bearing in mind that HoFeO_3 is characterized by

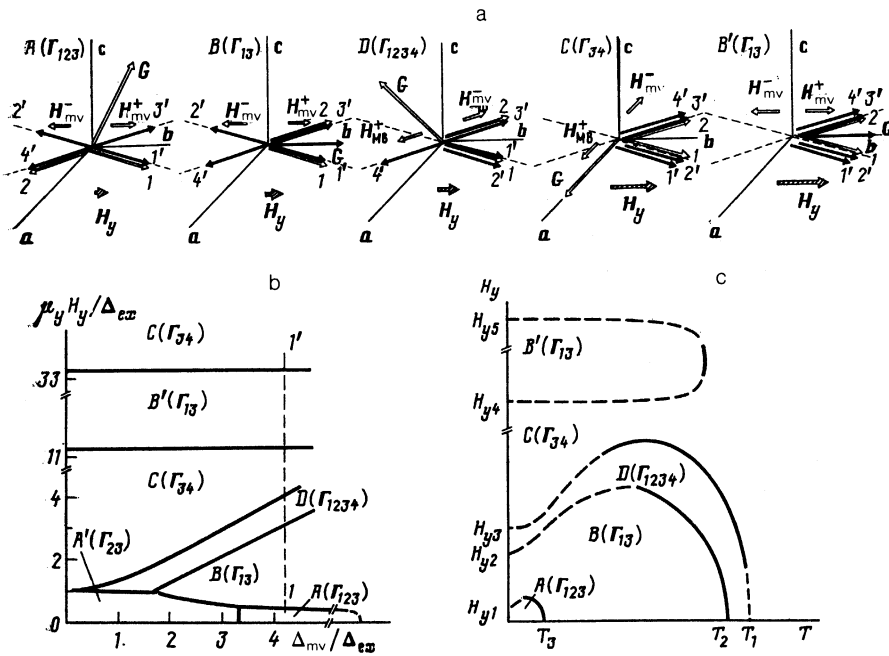


FIG. 8. Phase transitions in $\text{HoFe}_{1-x}\text{Al}_x\text{O}_3$ subjected to magnetic fields $\mathbf{H}\parallel\mathbf{b}$: a) magnetic configurations realized along the 1-1' magnetic path in Fig. 8b; b) phase diagram in the space defined by the external field ($\mu_y H_y / \Delta_{ex}$) and the field of the magnetic vacancies ($\Delta_{mv} / \Delta_{ex}$); c) H_y - T phase diagram where the continuous curves represent second-order phase transitions and the dashed curves represent first-order transitions.

$\Delta_{ex} = 4.7$ K and $\Delta_{qd} = 2.4$ K (Ref. 6), we find from the stability condition at $T = 0$ K of the A (Γ_{12}) phase of a sample with the $x = 0.03$ composition that Δ_{mv} obeys $14 \text{ K} \leq \Delta_{mv} \leq 32 \text{ K}$.

Let us now consider the magnetic-field-induced phase transitions.

Magnetic field $\mathbf{H}\parallel\mathbf{a}$

In this case the orientational phase transitions which occur in the investigated $\text{HoFe}_{1-x}\text{Al}_x\text{O}_3$ samples are the same as in pure HoFeO_3 , described in detail in Ref. 7. We therefore discuss them briefly. A characteristic feature of the H_x - T phase diagram of $\text{HoFe}_{1-x}\text{Al}_x\text{O}_3$ in the region of $T \sim 60$ K is (as in the case of HoFeO_3) a bicritical point Q (Figs. 3c and 5a) where the $\Gamma_{24}-\Gamma_2$ and $\Gamma_{12}-\Gamma_2$ second-order phase transition lines converge with the $\Gamma_{12}-\Gamma_{24}$ first-order transition line. The latter first-order transition has unfortunately not yet been observed experimentally, but this has been probably because of the weak anomaly of the magnetostriction and thermal expansion at this transition and also because of the inhomogeneity of the sample in question.

The low-temperature phase transitions in $\text{HoFe}_{1-x}\text{Al}_x\text{O}_3$ exhibit qualitatively new features associated with the magnetic vacancies. This is demonstrated by a change in the nature of the $\Gamma_{12}-\Gamma_2$ phase transition from the second to the first order, which is manifested at $T < T_{TK} \sim 8$ K by jumps in the magnetization curves (Fig. 3a). The jumps are due to an abrupt magnetization reversal experienced by some of the Ho^{3+} ions located near a magnetic vacancy which magnetizes these ions opposite to the external field. Such a magnetization reversal of some of the Ho^{3+} ions can be regarded as a special metamagnetic transition in the f subsystem, accompanied by reorientation of the antiferromagnetic vector \mathbf{G} of the Fe subsystem. The field for this transition at $T = 0$ K is

$$H_x^0 \approx [(\Delta_0 - \Delta_{ex}) / zx + \theta_x (1 - zx/2)] / \mu_x, \quad (16)$$

and the magnitude of the magnetization jump is $\Delta M_x \approx \mu_x zx$. For the sample with $x = 0.03$ this jump represents about one-quarter of the saturation magnetization μ_x , which is in agreement with the experimental results (Fig. 3a). If we assume that $\Delta_{ex} = 4.7$ K (Ref. 6), $\alpha \approx 65^\circ$, $\theta_x \approx 1$ K, and $\Delta_{mv} = 15$ K ($H_{mv} = 25$ kOe), we find that $H_x^0 \sim 6$ kOe for $x = 0.03$ and $H_x^0 = 17$ kOe for $x = 0.07$, in agreement with the experimental results (Figs. 3c and 5a).

Magnetic field $\mathbf{H}\parallel\mathbf{b}$

We shall first analyze the low-temperature phase transitions. Using Eqs. (8) and (14), we find that at $T = 0$ K the system can have the magnetic configurations listed below.

1) Phase A [Γ_{123} (G_{zy}, F_{xy})] has the same structure as in $H = 0$ (see Fig. 8a and the discussion above).

This phase is stable if

$$\mu_y H_y \leq \min \{ (\Delta_y^2 zx - \Delta_{ex}^2 (1 - zx)) / \Delta_0, \Delta_{ex} (1 - zx) / \Delta_0 \} + \theta_x (1 - zx). \quad (17)$$

2) Phase B [Γ_{13} (G_y, F_y)] is doubly degenerate and is characterized by

- a) $\mu_{1,4}' = \mu_0, \mu_{2,3}' = -\mu_0, \mu_1 = \mu_0, \mu_2 = -\mu_0, G_y = 1;$
- b) $\mu_{1,4}' = -\mu_0, \mu_{2,3}' = \mu_0, \mu_1 = \mu_0, \mu_2 = -\mu_0, G_y = -1.$

This phase is stable if $0 < \mu_y H_y < \Delta_y - (1 - zx) \theta_y$.

3) Phase D , which is quadruply degenerate, has the spatial orientation of the spins of the Fe subsystem (Γ_{1234} ($G_{x,y,z}, F_{x,y,z}$)), and is characterized by the following values of the variables:

- a) $\mu_{1,4}' = \mu_0, \mu_{2,3,4}' = -\mu_0, \mu_1 = \mu_0,$
 $\mu_2 = -\mu_0, \theta = \pi - \theta_1, \varphi = \alpha;$

$$b) \mu_2' = \mu_0, \mu_{1,3,4}' = -\mu_0, \mu_1 = \mu_0,$$

$$\mu_2 = -\mu_0, \theta = \pi - \theta_1, \varphi = \alpha + \pi;$$

$$c) \mu_3' = -\mu_0, \mu_{1,2,4}' = \mu_0, \mu_1 = \mu_0,$$

$$\mu_2 = -\mu_0, \theta = \theta_1, \varphi = -\alpha;$$

$$d) \mu_4' = -\mu_0, \mu_{1,2,3}' = \mu_0, \mu_1 = \mu_0,$$

$$\mu_2 = -\mu_0, \theta = \theta_1, \varphi = \pi - \alpha,$$

where θ and φ are the angles that determine the orientation of the \mathbf{G} vector, such that

$$\sin \theta_1 = \Delta_{mv} / \Delta, \quad \Delta = (\Delta_{ex}^2 + \Delta_{mv}^2)^{1/2}. \quad (18)$$

The range of stability of this phase is described by the interval

$$\max [(-\Delta_{mv}^2 \cos 2\alpha - \Delta_{ex}^2) / \Delta + 1/2zx\theta_x + (1 - 1/2zx)\theta_y; \Delta_{ex}^2 / \Delta - 1/2zx\theta_x + (1 - 1/2zx)\theta_y] < \mu_y H_y < [\Delta - 1/2zx\theta_x + (1 - 1/2zx)\theta_y]. \quad (19)$$

4) Phase C has the vector \mathbf{G} along the \mathbf{a} axis $[\Gamma_{34}(G_x, F_{y,z})]$. This phase is doubly degenerate ($G_x = \pm 1$) and its maximum magnetization is along the \mathbf{b} axis ($\mu_{1,2}' = \mu_1 = \mu_0, \mu_{3,4}' = \mu_2 = -\mu_0$) (Fig. 8a). This phase is stable if

$$H_y > \frac{\Delta_x + \theta_y}{\mu_y}, \quad (20a)$$

$$K_{ac}^0 > 0, \quad K_{ab}^0 + \chi_{\perp} (H_y + \bar{\mu}_y a)^2 > 0. \quad (20b)$$

It should be pointed out that the interaction of the antiferromagnetic vector \mathbf{G} with the f subsystem is suppressed in this phase, so that the orientation of this vector is governed by the other terms in the thermodynamic potential of Eq. (8), which are smaller than Δ_{mv} and Δ_{ex} : they are governed by the anisotropy constants ($K_{ab}^0, K_{ac}^0, K_2', K_2''$) and by the terms due to the tilt of the magnetic sublattices of the Fe subsystem ($\chi_{\perp} (H_y + \bar{\mu}_y a)^2$) which are strongly renormalized at low temperatures because of the isotropic R-Fe exchange.^{6,7,13}

5) Phase B' $[\Gamma_{13}(G_y, F_y)]$ (doubly degenerate, $G_y = \pm 1$), which is in contrast to phase B is characterized by the maximum magnetization along the \mathbf{b} axis ($\mu_{1,2}' = \mu_1 = \mu_0, \mu_{3,4}' = \mu_2 = -\mu_0$). This phase is stable if

$$H_y > \frac{\Delta_y + \theta_y}{\mu_y}, \quad (21a)$$

$$K_{bc}^0 - \chi_{\perp} (H_y + \bar{\mu}_y a)^2 > 0, \quad -K_{ab}^0 - K_2' - \chi_{\perp} (H_y + \bar{\mu}_y a)^2 > 0, \quad (21b)$$

where $(K_{bc}^0 = K_{ac}^0 + K_2'' - K_2')$.

Since the ranges of stability of the various phases overlap on the field scale, the phase transitions between them are first-order and the fields in which they are induced can be found by equating the thermodynamic potentials of the corresponding phases. A sequence of possible phase transitions can be represented conveniently in the phase diagram plotted in the space of H_y and Δ_{mv} , or in the space of the corresponding normalized quantities $\mu_y H_y / \Delta_{ex}$ and $\Delta_{mv} / \Delta_{ex}$. This diagram is plotted in Fig. 8b for $x = 0.03$ ($a = -140$

kOe, $H_{yf} = [-\frac{1}{2} K_{ab} - \frac{1}{4} K_2'] / \chi_{\perp}]^2 \approx 200$ kOe) ignoring the less important f - f interaction and the value of Δ_{qd} . If $\Delta_{mv} = 0$, it follows from Fig. 8b that an increase in the field induces the same sequence of the phase transitions as in pure holmium orthoferrite.¹³

An important special feature contributed by the magnetic vacancies ($\Delta_{mv} \neq 0$) is the existence, in a certain range of the phase D (Δ_{1234}) with the spatial orientation \mathbf{G} . It appears an increase in the field favors the transition from the low-field phases A (Γ_{13}) or A' (Γ_{23}) to the phase C (Γ_{34}) not by simultaneous magnetization reversal of the ions $2'$ and $4'$ (Fig. 8a) oriented by the field \mathbf{H}_{mv} against the external field, but by consecutive magnetization reversals accompanied by simultaneous rotation of \mathbf{H}_{mv} (or \mathbf{G}), when such magnetization reversal ends in a state in the space of the intermediate phase D in such a way that the projection of \mathbf{H}_{mv} along the magnetic moment of one of these ions ($2'$ or $4'$) decreases, whereas the projection along the magnetic moment of the other increases, so that magnetization reversal is facilitated in the former case and hindered in the latter case (this applies to the ions $2'$ and $4'$, respectively in Fig. 8a).

We should mention also the unusual nature of the $A(\Gamma_{123})-B(\Gamma_{13})$ phase transition, for which an increase in the field reorients the antiferromagnetic vector from the canted phase ($G_{z,y}$) to the G_y state ($\mathbf{G} \parallel \mathbf{H}_y$). The mechanism of this phase transition involves suppression, due to the additional splitting of the ground quasidoublet of the Ho^{3+} ion by an external field, of the "magnetic Jahn-Teller effect" mentioned above, which leads to the $\Gamma_1-\Gamma_{12}$ spontaneous transition as a result of cooling.

In relatively strong fields the system can undergo the reverse spin-flop transition $C(\Gamma_{34})-B'(\Gamma_{13})$ which is due to the action on the Fe^{3+} ion spins not only of the external field, but also of the negative effective field due to the isotropic f - d exchange ($a < 0$).¹²

It should be noted that in even stronger fields we can expect the usual $B'(\Gamma_{13})-C(\Gamma_{34})$ spin-flop transition.

It therefore follows that an increase in the field applied to the $\text{HoFe}_{1-x}\text{Al}_x\text{O}_3$ system should induce at least five phase transitions (as demonstrated by the thermodynamic path 1-1' in Fig. 8b). The fields for these transitions are as follows:

$$\begin{aligned} A \rightarrow B: \quad H_{y1} &= [(\Delta_0 - \Delta_y z x) / (1 - z x) + 1/2 (1 - z x) (\theta_y - \theta_x)] / \mu_y, \\ B \rightarrow D: \quad H_{y2} &= [(2\Delta_y - \Delta) + (1 - 3/4 z x) \theta_y + 1/4 z x \theta_x] / \mu_y, \\ D \rightarrow C: \quad H_{y3} &= [(\Delta + (1 - 1/4 z x) \theta_y - 1/4 z x \theta_x)] / \mu_y. \end{aligned} \quad (22)$$

The first three transitions should be accompanied by the following magnetization jumps in the Ho subsystem:

$$\begin{aligned} C \rightarrow B': \quad H_{y4} &= -a \bar{\mu}_y - H_{sf}, \\ B' \rightarrow C: \quad H_{y5} &= -a \bar{\mu}_y + H_{sf}. \end{aligned}$$

The magnetization curve along the \mathbf{b} axis (Fig. 1a), however, does not exhibit these jumps; this is clearly due to the broadening of the transitions related to the finite temperatures and the wide range of existence of the intermediate state, since the corresponding demagnetization factor of a sample is $N_y \sim 4\pi$. On the other hand, the magnetostriction isotherms (Fig. 6) demonstrate clearly a number of anomalies which can be attributed in a natural manner to these

phase transitions. A small anomaly at $H_y \sim 5$ kOe for the $x = 0.03$ composition (Fig. 6b) can be attributed to the $A(\Gamma_{123})-B(\Gamma_{13})$ phase transition. Note that in the case of the composition with $x = 0.07$, for which the spontaneous canted phase Γ_{12} is absent at low temperatures, there is no such anomaly in the magnetostriction. The remaining anomalies of the magnetostriction observed for both observations in fields within the interval 7–25 kOe (Fig. 6a) can be interpreted as $B(\Gamma_{13})-D(\Gamma_{1234})-C(\Gamma_{34})$ phase transitions. A more detailed analysis is difficult because of the broadening of the transitions by the large demagnetization factor.

If we assume that $\Delta_{ex} = 4.7$ K (Ref. 6), $\theta_x \sim \theta_y \sim K$, $\Delta_{mv} \approx 15$ K ($H_{mv} \sim 25$ kOe), we find that the fields for these transitions in the case of a sample with $x = 0.03$ are as follows: $H_{y1} \sim 4$ kOe, $H_{y2} \sim 23$ kOe, and $H_{y3} \sim 31$ kOe; for a sample with a higher aluminum concentration ($x = 0.07$), which does not undergo the $A-B$ transition, the fields H_{y2} and H_{y3} are practically the same, which is on the whole in reasonable agreement with the experimental data (Fig. 6).

At finite temperatures the results of an analysis of the stability of the magnetic configurations of the system can be represented in the form of the H_y-T phase diagram deduced from the thermodynamic potential of Eq. (8) and plotted in Fig. 8c. We can see that an increase in temperature modifies the nature of the phase transition from the first- to the second-order and the corresponding fields depend strongly on the temperature of a sample.

CONCLUSIONS

Our investigation of the magnetic and magnetoelastic properties of the $\text{HoFe}_{1-x}\text{Al}_x\text{O}_3$ system demonstrates that the magnetic vacancies induce not only a new (compared with pure HoFeO_3) spontaneous spin-reorientation transitions ($\Gamma_4 - \Gamma_{12} - \Gamma_1 - \Gamma_{12}$ for $x = 0.03$ and $\Gamma_4 - \Gamma_{12} - \Gamma_1$ for $x = 0.07$), but also unusual phase transitions in an external magnetic field. A characteristic feature of these transitions in a field at low temperatures is associated with the presence of characteristic metamagnetic transitions in the f subsystem, which are due to the abrupt magnetization reversal exhibited by those rare-earth ions whose environment contains a magnetic vacancy which magnetizes these ions against the external magnetic field. The $f-d$ exchange interaction ensures that these metamagnetic transitions induce spin-reorientation transitions in the d subsystem, i.e., the latter effectively occur in an external exchange field and are not due to the direct effect of the external field on the d subsystem. This d subsystem in turn governs the effective fields at the rare-earth ions and strongly influences the threshold fields of the corresponding phase transitions.

In the $\text{HoFe}_{1-x}\text{Al}_x\text{O}_3$ system we have investigated these characteristics appear fully in external magnetic fields $\mathbf{H}\parallel\mathbf{a}$ and $\mathbf{H}\parallel\mathbf{b}$. For $\mathbf{H}\parallel\mathbf{a}$, such a metamagnetic transition in the Ho subsystem is accompanied by the $\Gamma_{12}(G_y G_z F_x) - \Gamma_2(G_z F_x)$ spin-reorientation transition in the d subsystem which is manifested by a jump of the magnetization and magnetostriction curves. A characteristic feature of our H_x-T phase diagram is the existence of a bicritical point at $T \sim 60$ K where two lines of the second-order ($\Gamma_2-\Gamma_{12}$ and $\Gamma_{24}-\Gamma_2$) phase transition converge with the first-order ($\Gamma_{24}-\Gamma_{12}$) phase transition line.

For $\mathbf{H}\parallel\mathbf{b}$ then at low temperatures the phase transitions are much more complex than in $\mathbf{H}\parallel\mathbf{a}$.

Firstly, in the case of the $x = 0.03$ position which exhibits the canted phase Γ_{12} at temperatures $T < 8$ K for $H = 0$, in relatively weak fields $\mathbf{H}\parallel\mathbf{b}$ ($H \sim 5$ kOe), there is an unusual $\Gamma_{123}(G_y F_x G_z F_y) - \Gamma_{13}(G_y F_y)$, phase transition, i.e., a transition to a state with the antiferromagnetic vector \mathbf{G} parallel exactly to the external fields. The mechanism of this special phase transition involves suppression, by the external field $\mathbf{H}\parallel\mathbf{b}$, of the magnetic Jahn-Teller effect, which is the cause of the appearance of the spontaneous Γ_{12} phase.

Secondly, in stronger $\mathbf{H}\parallel\mathbf{b}$ fields both the investigated compositions exhibit two additional phase transitions ($\Gamma_{13} - \Gamma_{1234} - \Gamma_{34}$), which are due to consecutive magnetization reversal of the rare-earth ions at inequivalent positions, magnetized by the effective field of the magnetic vacancies against the external magnetic field, and accompanied by reorientation of the vector \mathbf{G} from the \mathbf{b} axis [$\Gamma_{13}(G_y)$ phase] to the \mathbf{a} axis [$\Gamma_{34}(G_x)$] via an intermediate phase ($\Gamma_{1234}(G_x G_y G_z)$). The theoretical $H-T$ phase diagram plotted for $\mathbf{H}\parallel\mathbf{b}$ agrees on the whole with the experimental results and predicts that in stronger fields ($H > 100$ kOe) a reverse spin-flop transition ($\Gamma_{34}-\Gamma_{13}$) should be followed by the usual spin-flop transition ($\Gamma_{13}-\Gamma_{34}$).

¹ It should be pointed out that the magneto-optic measurements were used not quite accurately in Ref. 9 to label the magnetic phases that appear in $\text{HoFe}_{1-x}\text{Al}_x\text{O}_3$: $\Gamma_2-\Gamma_1-\Gamma_2-\Gamma_{24}-\Gamma_4$.

² The low-field inflection of the magnetization isotherm is due to a transition to a single-domain state in the Γ_{12} phase, whereas the high-field anomaly is due to the $\Gamma_{12}-\Gamma_2$ phase transition. The coordinates of the high-field anomaly are represented by a point in the experimental $H-T$ phase diagram.

¹ A. K. Zvezdin, A. M. Kadomtseva, and A. A. Mukhin, *Izv. Akad. Nauk SSSR Ser. Fiz.* **44**, 1348 (1980).

² A. M. Kadomtseva, A. K. Zvezdin, M. M. Lukina *et al.*, *Zh. Eksp. Teor. Fiz.* **73**, 2324 (1977) [*Sov. Phys. JETP* **46**, 1216 (1977)].

³ K. P. Belov, A. K. Zvezdin, A. M. Kadomtseva, and R. Z. Levitin, *Oriental Transitions in Rare-Earth Magnetic Materials* [in Russian], Nauka, Moscow (1979).

⁴ V. N. Derkachenko, A. K. Zvezdin, A. M. Kadomtseva *et al.*, *Phys. Status Solidi A* **84**, 215 (1984).

⁵ I. A. Zorin, A. M. Kadomtseva, I. B. Krynetskiĭ *et al.*, *Fiz. Tverd. Tela* (Leningrad) **30**, 76 (1988) [*Sov. Phys. Solid State* **30**, 41 (1988)].

⁶ A. M. Balbashov, G. V. Kozlov, S. P. Lebedev *et al.*, *Zh. Eksp. Teor. Fiz.* **95**, 1092 (1989) [*Sov. Phys. JETP* **68**, 629 (1989)].

⁷ G. P. Vorob'ev, A. M. Kadomtseva, I. B. Krynetskiĭ, and A. A. Mukhin, *Zh. Eksp. Teor. Fiz.* **95**, 1049 (1989) [*Sov. Phys. JETP* **68**, 604 (1989)].

⁸ I. A. Zorin, A. M. Kadomtseva, M. M. Lukina, and A. A. Mukhin, *Zh. Eksp. Teor. Fiz.* **93**, 266 (1987) [*Sov. Phys. JETP* **66**, 153 (1987)].

⁹ K. Piotrowski, R. Szymczak, V. V. Ermenko *et al.*, *Acta. Phys. Pol. A* **72**, 343 (1987).

¹⁰ A. K. Zvezdin and V. M. Matveev, *Zh. Eksp. Teor. Fiz.* **77**, 1076 (1979) [*Sov. Phys. JETP* **50**, 543 (1979)].

¹¹ V. G. Bar'yakhtar, A. E. Borovik, and V. A. Popov, *Zh. Eksp. Teor. Fiz.* **9**, 634 (1969) [*Sov. Phys. JETP* **9**, 391 (1969)].

¹² G. P. Vorob'ev, A. M. Kadomtseva, I. B. Krynetskiĭ, and A. A. Mukhin, *Zh. Eksp. Teor. Fiz.* **98**, 1726 (1990) [*Sov. Phys. JETP* **71**, 969 (1990)].

¹³ A. K. Zvezdin, V. M. Matveev, A. A. Mukhin, and A. I. Popov, *Rare-Earth Ions in Magnetically Ordered Crystals* [in Russian], Nauka, Moscow (1985).

Translated by A. Tybulewicz